specimens CIP-R and PC2-R, 33% and 40% of the original steel elastic modulus were used to model the damaged steel, correspondingly. Secondly, a one-dimensional bond-slip model, as shown in Fig. 4(b), based on recent research [22] was modified for the repaired specimen. In the bond-slip model, as shown in Fig. 4(b), the longitudinal steel bar with the damaged steel properties was discretized and connected to the bond-slip springs, which were modeled using the ZeroLength Element. The bond stress-slip relationships in the bond-slip springs were obtained from the CEB-FIB Code in the case of splitting mode failure[17]. For the length of the steel bar embedded in the previously damaged region, the bond stress-slip relationship for unconfined concrete was used for the bond-slip spring elements; for the remaining length of the steel bar outside the previously damaged region, the bond stress-slip relationship for confined concrete was used for the bond-slip spring elements. In the one-dimensional bond-slip model, one end of the steel bar was pulled to get the total deformation, including both steel bar elongation and slip.

The total deformation of the steel bar, Δs, including both elongation and slip was obtained. The strain, ε, was calculated based on Eq. (2):

$$\varepsilon = \frac{\Delta_s}{L_{pl}} \tag{2}$$

where L_{pl} is the defined plastic hinge length. In Model Fiber, 356 mm (14 in.), or 67% of the column width, was used for the defined plastic hinge length of cast-in-place specimen CIP-R; a defined plastic hinge length of 305 mm (12 in.), or 57% of the column width, was used for precast concrete specimen PC2-R. The modified steel stress-strain curve with consideration of initial damage and bond-slip is thus obtained, which was used for the steel bars in the plastic hinge region of Model Fiber.

Model rotational spring (RS)

In Model RS, concentrated plasticity was considered using a non-linear moment rotational spring located at the repaired cross-section. A sectional moment-curvature analysis was performed, based on damaged steel properties and considering bond slip, to obtain the moment-rotation relationship, which is assigned to the non-linear rotational spring. The model with a rotational spring, referred to as Model RS, is shown in Fig. 5(a). For this nonlinear rotational spring, a moment-rotation curve is considered as the input, as shown in Fig. 5(b) [21,22]. The *Hysteretic* material in *OpenSees* is used to represent moment-rotation relationships with the selected parameter as shown in Table 2. The moment-rotation at the peak point was derived from sectional analysis considering bond-slip.

COMPARISON OF ANALYTICAL AND EXPERIMENTAL RESULTS

The results for repaired specimens CIP-R and PC2-R from Model Fiber and Model RS are compared to the experimental results in terms of hysteretic response, hysteretic energy, and moment-rotation relationship in Figs. 6-9. Both Model Fiber and Model RS predict the backbone curve and hysteretic energy in a satisfactory manner. For specimen CIP-R, Model Fiber performed better than Model RS at capturing the pinching behavior of the hysteresis, as shown by comparing Fig. 6(a) to 6(b). For specimen PC2-R, Model RS performed better than Model Fiber for matching the experimental hysteresis curve, as shown by comparing Fig. 8(a) to 8(b). Regarding moment-rotation at the repaired section, the experimental moment-rotation curve was measured up to the peak bending moment, as shown in Figs. 7 and 9. The analytical results for Model RS and Model Fiber not only matched the experimental results, but also predicted the performance after softening. Comparisons between experimental and analytical results in terms of hysteretic energy for specimen CIP-R and PC2-R are shown in Figs. 7(a) and 9(a). The results from the two analytical models agree well with the experimental results.

Low-cycle fatigue of column longitudinal steel bars in Model Fiber is also predicted. For specimen PC2-R, extreme longitudinal bars fractured in the last cycle due to low-cycle fatigue, at the specific drift ratios shown in Fig. 8(a); this shows very good agreement with the experimental results [7,8]. For the analysis of specimen CIP-R with pinching and bond-slip due to debonding between the column and repair system, Model Fiber would be more appropriate than Model RS for simulating the structural behavior. For structures without significant bond-slip between steel bars and surrounding concrete, and for precast concrete structures, Model RS would be preferable.

CONCLUSIONS

Two severely damaged bridge columns, with damage including bar pullout, buckling and fracture of column longitudinal steel reinforcing bars, and considerable concrete crushing, were successfully repaired. A steel collar was provided to increase the bond between the original column concrete and the external CFRP shell with anchored headed steel bars and non-shrink grout. The following conclusions can be made:

1. The proposed repair method of using a CFRP shell and epoxy anchored headed steel bars effectively relocated the column plastic hinge; strength capacity, displacement capacity, and energy dissipation were successfully restored. The steel collar was successful in strengthening the bond between original column concrete and repair concrete.

2. Two analytical models, the first considering plasticity spread over a defined plastic hinge length (Model Fiber) and the second using a concentrated rotational spring (Model RS), reproduced hysteresis curves and hysteretic energy dissipation that matched the experimental results very well.

3. Both Model Fiber and Model RS analytical models considered bond-slip effects, effects of previous loading history and degradation of longitudinal steel bars, and low-cycle fatigue effects.

4. Model Fiber is easier to implement than Model RS; the latter specifically requires the moment versus rotation properties of the nonlinear spring as input.

5. Model Fiber performed better than Model RS for matching hysteresis curves, especially for structures with a pinching effect. The proposed analytical model, Model Fiber, in addition to matching the hysteresis curves produced local responses such as moment-rotation relationships and could be used for prediction purposes.

6. Model RS performed better than Model Fiber for matching the hysteresis curves of precast concrete structures that have a good bond condition between column longitudinal bars and column concrete, as well as between column concrete and CFRP donut concrete.

ACKNOWLEDGEMENTS

The authors would like to acknowledge the financial support of the Mountain Plains Consortium under contract MPC-491. In addition, they would like to acknowledge the support of MJ Ameli, Mark Bryant, Priyank Sankholkar, Trevor Nye, Anurag Upadhyay, and Joel Parks of the Department of Civil and Environmental Engineering at the University of Utah.

NOTATION

a_s = coefficient about if the bond-slip is considered in the plastic hinge
d_b = diameter of the longitudinal column reinforcement
f_y = yield strength of the steel bars
L_{pl} = plastic hinge length
L_s = shear span
ε = strain of longitudinal bars
Δ_s = total deformation of the steel bar

REFERENCES

[1] M. J. N. Priestley, F. Seible, Y. Xiao, and R. Verma, "Steel jacket retrofitting of reinforced concrete bridge columns for enhanced shear strength-Part 1: Theoretical considerations and test design," *ACI Struct. J.*, vol. 91, no. 4, pp. 394–405, 1994.

[2] F. Seible, M. J. N. Priestley, G. A. Hegemier, and D. Innamorato, "Seismic Retrofit of RC Columns with Continuous Carbon Fiber Jackets," *J. Compos. Constr.*, vol. 1, no. 2, pp. 52–62, 1997.

[3] J. Gergely, C. P. Pantelides, and L. D. Reaveley, "Shear Strengthening RCT-joints Using CFRP Composites," *J. Compos. Constr.*, vol. 4, no. 2, pp. 56–64, 2000.

[4] C. P. Pantelides, J. B. Duffin, and L. D. Reaveley, "Seismic Strengthening of Reinforced-Concrete Multicolumn Bridge Piers," *Earthq. Spectra*, vol. 23, no. 3, pp. 635–664, 2007.

[5] J. E. Parks, D. N. Brown, M. J. Ameli, and C. P. Pantelides, "Seismic repair of severely damaged precast reinforced concrete bridge columns connected with grouted splice sleeves," *ACI Struct. J.*, vol. 113, no. 3, pp. 615–626, 2016.

[6] R.-Y. Wu and C. P. Pantelides, "Rapid seismic repair of severely damaged cast-in-place reinforced concrete bridge piers (No. 17-06278)," 2017.

[7] R.-Y. Wu and C. P. Pantelides, "Rapid Seismic Repair of Severely Damaged Reinforced Concrete Bridge Piers," in *Structures Congress 2017*, 2017, pp. 370–381.

[8] R.-Y. Wu and C. P. Pantelides, "Rapid Repair and Replacement of Earthquake-damaged Concrete Columns Using Plastic Hinge Relocation," *Compos. Struct.*, vol. 180, pp. 467–483, 2017.

[9] R.-Y. Wu and C. P. Pantelides, "Rapid Seismic Repair of Reinforced Concrete Bridge Columns," *ACI Struct. J.*, vol. 114, no. 5, pp. 1339–1350, 2017.

[10] AASHTO, *AASHTO guide specifications for LRFD seismic bridge design*, 2nd ed. Washington D.C.: American Association of State Highway and Transportation Officials, 2011.

[11] M. J. Ameli, J. E. Parks, D. N. Brown, and C. P. Pantelides, "Seismic evaluation of grouted splice sleeve connections for reinforced precast concrete column–to–cap beam joints in accelerated bridge construction," *PCI J.*, vol. 60, no. 2, pp. 80–103, 2015.

[12] T. B. Panagiotakos and M. N. Fardis, "Deformation of reinforced concrete members at yielding and ultimate," *ACI Struct. J.*, vol. 98, no. 2, pp. 135–148, 2001.

[13] R. Eligehausen, E. P. Popov, and V. V. Bertero, "Local Bond Stress-Slip Relationships of Deformed Bars under Generalized Excitations," *Proc. 7th Eur. Conf. Earthq. Eng.*, pp. 69–80, 1982.

[14] J. Zhao and S. Sritharan, "Modeling of Strain Penetration Effects in Fiber-Based Analysis of Reinforced Concrete StructuresConcrete Structures," *ACI Struct. J.*, vol. 104, no. 2, pp. 133–141, 2007.

[15] S. Mazzoni, F. McKenna, M. H. Scott, and G. L. Fenves, *OpenSees Command Language Manual*. Berkely, California: Pacific Earthquake Engineering Research Center, 2007.

[16] F. Braga, R. Gigliotti, M. Laterza, M. D. Amato, and S. Kunnath, "Modified Steel Bar Model Incorporating Bond-Slip for Seismic Assessment of Concrete Structures," *J. Struct. Eng.*, vol. 138, no. November, pp. 1342–1350, 2012.

[17] CEB-FIP, *CEB-FIP Model Code 1990*. Thomas Telford Ltd., London, 1993.

[18] A. Vosooghi and M. S. Saiidi, "Design guidelines for rapid repair of earthquake-damaged circular RC bridge columns using CFRP," *J. Bridg. Eng.*, vol. 18, no. 9, pp. 827–836, 2013.

[19] M. H. Scott and G. L. Fenves, "Plastic Hinge Integration Methods for Force-Based Beam–Column Elements," *J. Struct. Eng.*, vol. 132, no. 2, pp. 244–252, 2006.

[20] P. Uriz, "Towards Earthquake Resistant Design of Concentrically Braced Steel Structures," University of California, Berkeley, 2005.

[21] R.-Y. Wu and C. P. Pantelides, "Concentrated and Distributed Plasticity Models for Seismic Repair of Damaged RC Bridge Columns," *J. Compos. Constr.*, vol. 22, no. 5, p. 04018044, 2018.

[22] M. J. Ameli and C. P. Pantelides, “Seismic analysis of precast concrete bridge columns connected with grouted splice sleeve connectors,” *J. Struct. Eng.*, vol. 143, no. 2, p. 04016176:1-13, 2016.

[23] C. B. Haselton, A. B. Liel, S. C. Taylor-Lange, and G. G. Deierlein, “Calibration of Model to Simulate Response of Reinforced Concrete Beam-Columns to Collapse,” *ACI Struct. J.*, vol. 113, no. 6, pp. 1141–1152, 2016.

[24] L. F. Ibarra and H. Krawinkler, “Global Collapse of Frame Structures under Seismic Excitations,” Berkeley, California, 2005.

Table 1—Original and repaired specimen test results

Specimen	CIP-O	CIP-R	PC2-O	PC2-R
Lateral load capacity, kN (kip)	168 (37.8)	203 (45.6)	177 (39.7)	217 (48.8)
Ultimate drift ratio, (%)	9.3	8.1	5.5	7.6
Failure mode	East and west bar fracture	Severe concrete crushing	GSS bar pullout	West and east bar fracture
Displacement ductility	9.9	6.8	4.9	7.1

Table 2 — Parameters used in hysteretic material of Model RS

Specimen	Pinching factor for force, $\boldsymbol{p_x}$	Pinching factor for deformation, $\boldsymbol{p_y}$	Damage due to ductility, $\boldsymbol{D_1}$	Damage due to energy, $\boldsymbol{D_2}$	Unloading stiffness degradation factor, $\boldsymbol{\beta}$
CIP-R	0.45	0.20	0.004	0.02	0.30
PC2-R	1.00	1.00	0.000	0.01	0.35

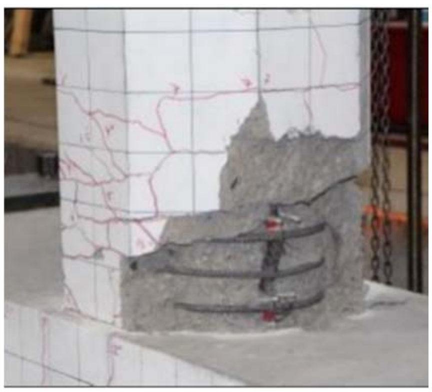

(a)

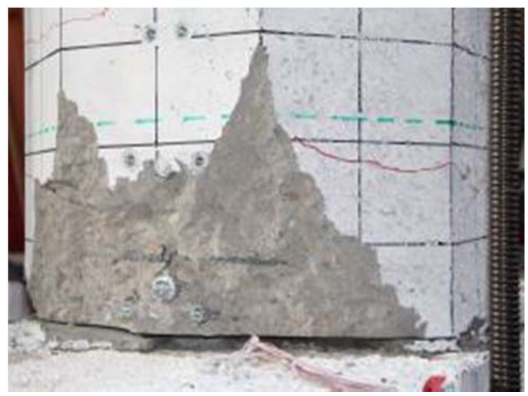

(b)

Fig. 1—Original specimen damage: (a) CIP-O; (b) PC2-O

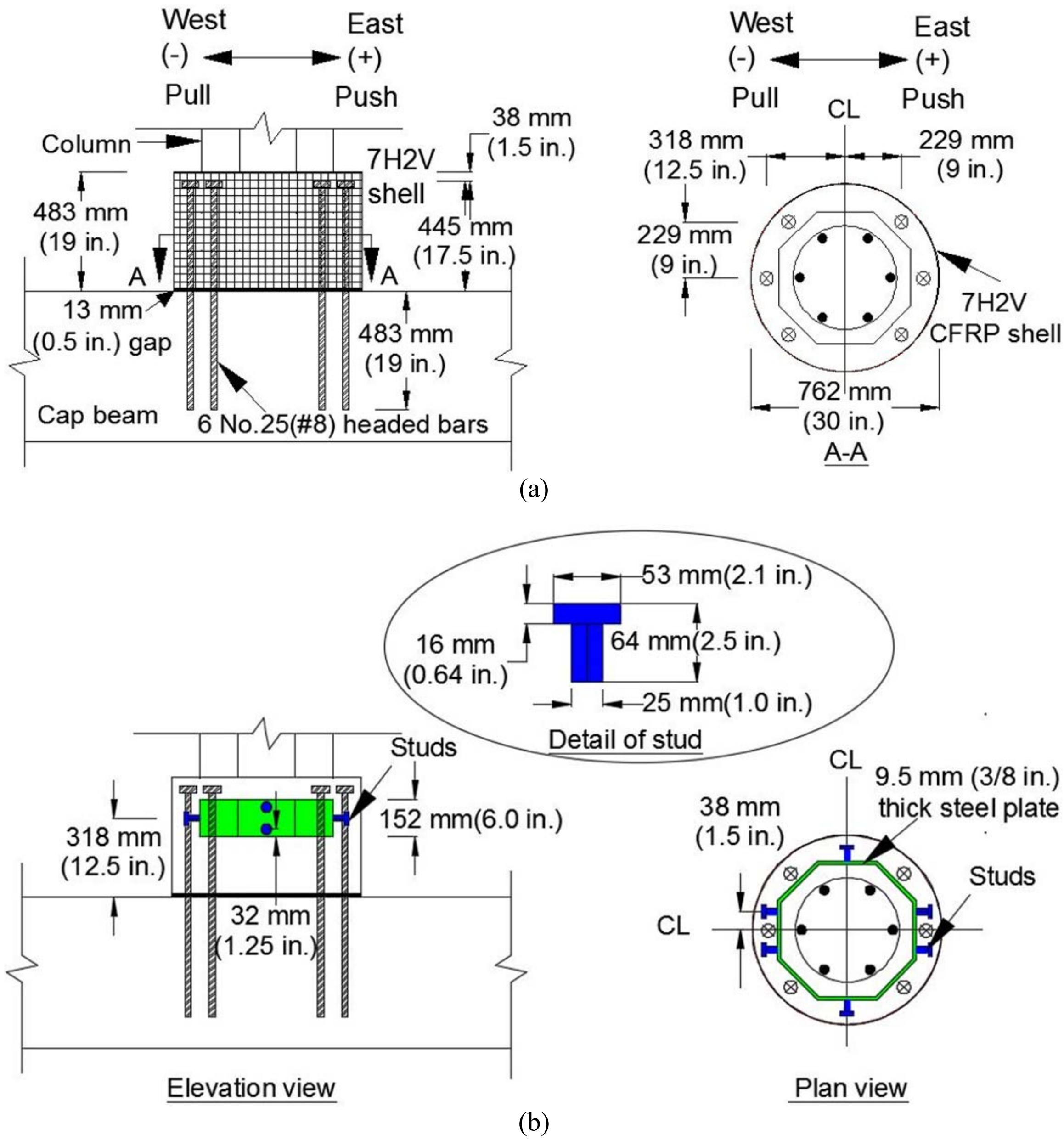

Fig. 2—Repair design: (a) CFRP donut design for CIP-R and PC2-R; (b) steel collar design for PC2-R

(a) (b)

Fig. 3—Plastic hinge relocation: (a) CIP-R; (b) PC2-R

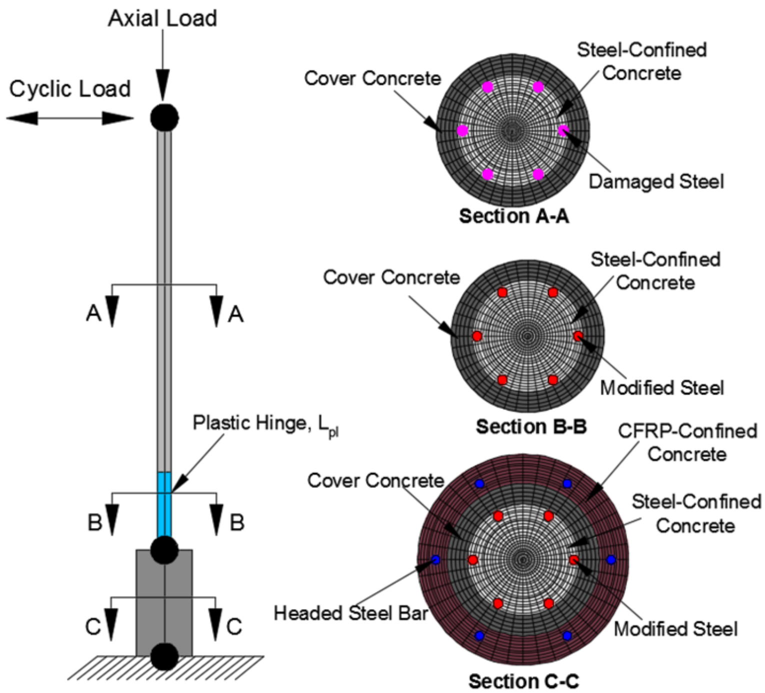

(a)

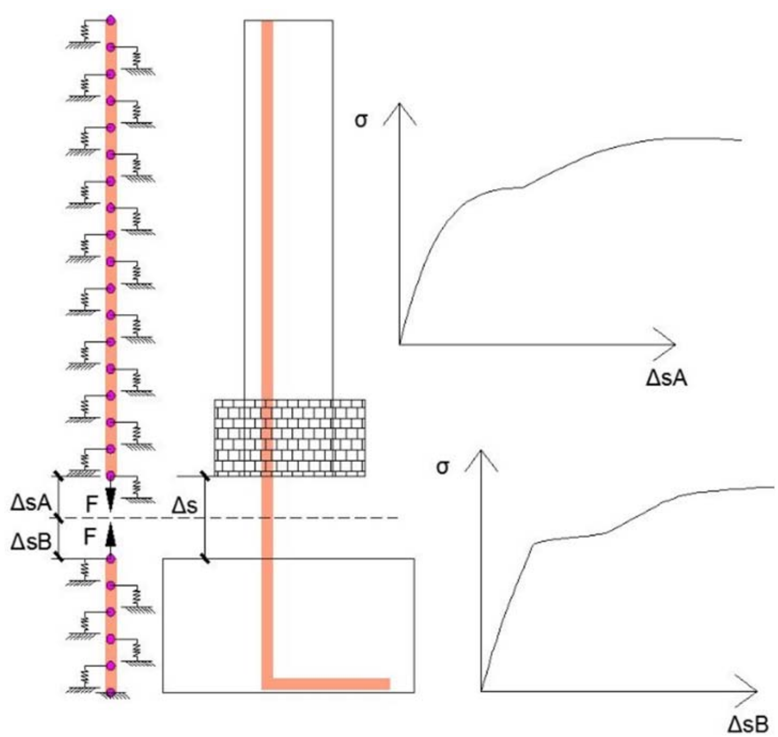

(b)

Fig. 4—Model Fiber: (a) schematic of Model Fiber; (b) schematic of bond-slip model

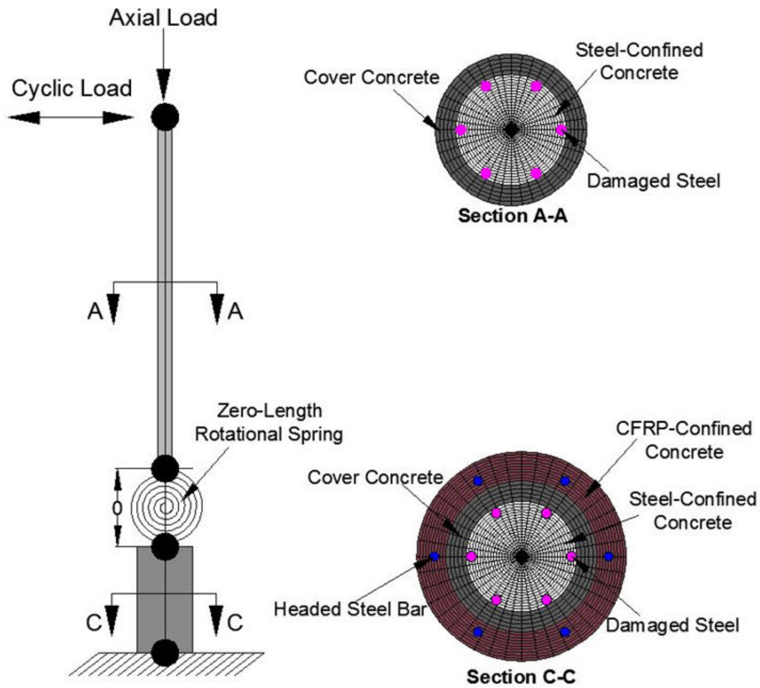

(a)

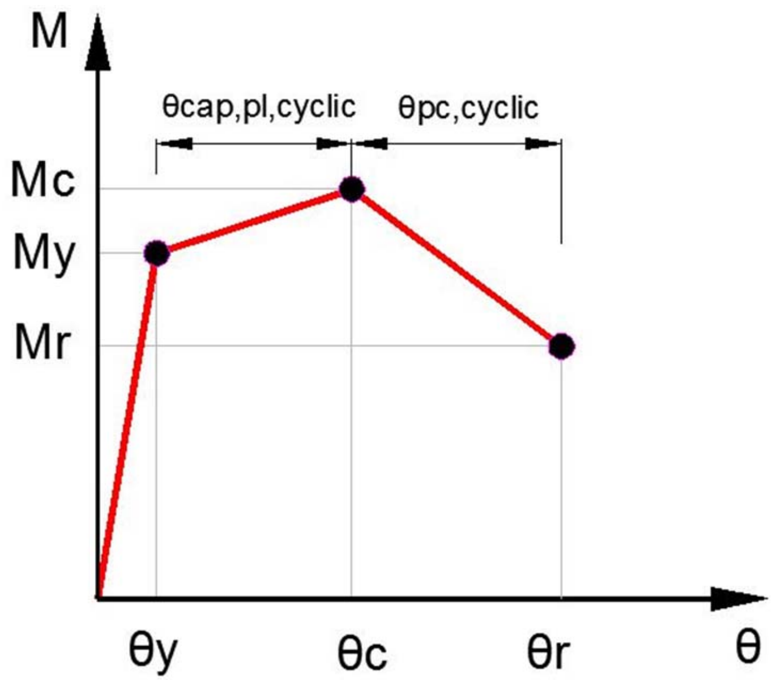

(b)

Fig. 5—Model RS: (a) schematic of Model RS; (b) backbone curve for rotational spring

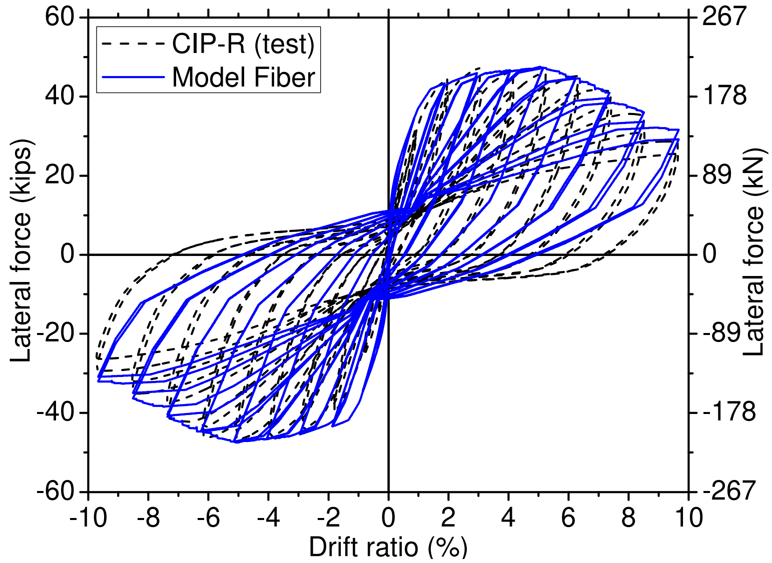

(a)

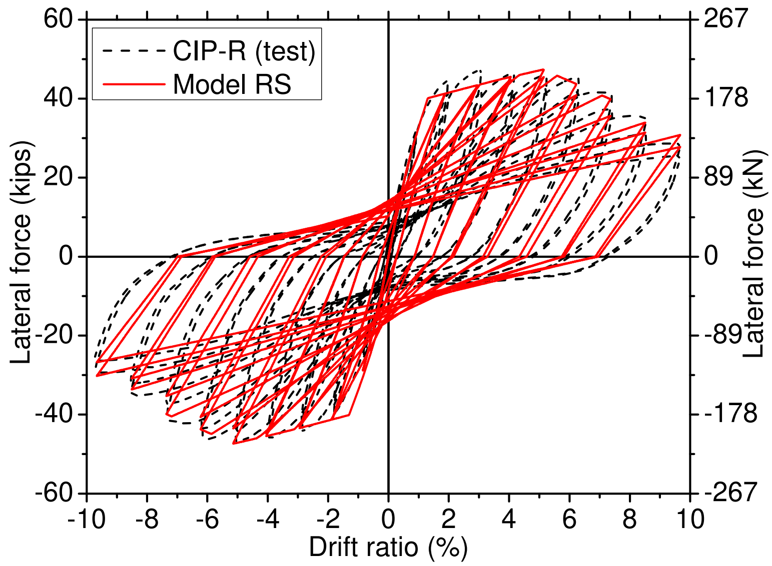

(b)

Fig. 6—Hysteretic response of CIP-R: (a) Model Fiber and test; (b) Model RS and test